Assembling and compressing a semifluorinated alkane monolayer on a hydrophobic surface: Structural and dielectric properties

Abdel I. El Abed* and Radoslav Ionov
Laboratoire de Neuro-Physique Cellulaire, Université René Descartes, 45 rue des Saints-Pères, 75006 Paris, France

Mohamed Daoud
Laboratoire de Mécanique, Matériaux et Procédés, ESSTT, 5 Av. Taha Hussin, Tunis, Tunisia

Olivier Abillon
Laboratoire de Physique Statistique, Ecole Normale Supérieure, 24 rue Lhomond, 75005 Paris, France
(Received 29 March 2004; published 23 November 2004)

We investigate the dynamic behavior upon lateral compression of a semifluorinated alkane $F(CF_2)_8(CH_2)_{18}H$ (denoted F_8H_{18}), spread on the hydrophobic top of a suitable amphiphilic monolayer: namely, a natural α-helix alamethicin peptide (alam). We show, in particular, the formation of an asymmetric flat bilayer by compressing at the air-water interface a mixed Langmuir film made of F_8H_{18} and alam. The particular chemical structure of F_8H_{18}, the suitable structure of the underlying alam monolayer and its collapse properties, allow for a continuous compression of the upper F_8H_{18} monolayer while the density of the lower alam monolayer remains constant. Combining grazing incidence x-ray reflectivity, surface potential, and atomic force microscopy data allow for the determination of the orientation and dielectric constant of the upper F_8H_{18} monolayer.

DOI: 10.1103/PhysRevE.70.051607 PACS number(s): 68.18.−g, 61.10.Kw, 68.55.Jk, 61.30.−v

I. INTRODUCTION

In spite of their simple chemical structure, semifluorinated *n*-alkanes $F(CF_2)_n(CH_2)_mH$ (denoted F_nH_m or SFA) can exhibit a large variety of stable smectic and lamellar phases [1–4] which generally cannot be described accurately by simple molecular models. The complex phase behavior of such molecules is mainly due to the presence in the same molecule of two "mutually phobic" —$(CH_2)_n$— and —$(CF_2)_n$— blocks and to a large difference in their chains cross sections—i.e., 0.28 nm^2 for —$(CF_2)_n$— and 0.18 nm^2 for —$(CH_2)_n$—.

An interesting feature of SFA, which is inherent to the presence of both oleophilic and oleophobic chains, is their ability to exhibit surface activity at the liquid alkane-air interface [5–8]. However, since the free energy of transfer of one —CH_2— group from an alkane solvent to a perfluorinated alkane solvent (1.1 kJ mol^{-1}) is only one-third the energy needed to transfer a —CH_2— group from an alkane solvent to water [6], attempts to study the dynamic properties of SFA monolayers upon compression at the liquid alkane-air interface, in the same manner as for classical amphiphilic Langmuir films [9], have failed. Instead, some SFA can form stable monolayers at the air-water interface which can be compressed to relatively high surface pressures, as shown initially by Gaines in 1992 [5] and studied in more detail later by Huang *et al.* [10], El Abed *et al.* [11,12], and Maaloum *et al.* [13] (see for a recent review Ref. [14]).

We show in this paper that, since some SFA can form monolayers either on the water or on oil-like surfaces, an alternative way to study the dynamic behavior of SFA monolayers on hydrophobic surfaces can be achieved through the spreading at the air-water interface of mixtures of SFA with a suitable amphiphilic material. We show, in particular, the spontaneous spreading of F_8H_{18} molecules on the top of Langmuir monolayer made of a natural amphiphilic rodlike molecule: α-helix alamethicin peptide (alam). The two-dimensional (2D) crystalline structure and the suitable collapse properties of the underlying alam monolayer allow for a continuous compression of the F_8H_{18} monolayer on the top of the underlying monolayer whose density remains constant.

Surface pressure (π) versus molecular area *A* and grazing-incidence x-ray reflectivity (GIXR) measurements show that the observed dense phase of the semifluorinated monolayer may consist of either a parallel or an antiparallel molecular organization. Additional atomic force microscopy (AFM) observations and surface potential (ΔV) versus molecular area *A* measurements allow for discrimination between these two possible orientations and also for the determination of the dielectric constant of the semifluorinated monolayer value.

II. EXPERIMENT

The rodlike α-helix alamethicin is a natural antibiotic peptide constituted by 19 amino-acid residues and one amino alcohol. The biological property of alamethicin relies on its amphiphilic feature and its ability to form ionic channels across the biological cell membrane. The majority of the alamethicin amino-acid residues, including the N-terminus, are hydrophobic in nature. The peptide is amphiphilic since its polar hydrophilic groups are either at the C-terminus or lies along a narrow hydrophilic strip parallel to the helix

*Electronic address: abdel.el-abed@univ-paris5.fr

axis. The used alamethicin compound was purchased from Sigma (Mw. 1959.9) and used as received.

The used F_8H_{18} compound was synthesized and purified (>98%) according to a well-known procedure [1]. At ambient temperature, it exhibits a crystalline phase which melts to an isotropic liquid at a temperature equal to 53 °C. The length of the fluorinated blocks can be evaluated from literature data [3,15] using this formula: L_F (nm) $=0.13(n-1)+0.238\approx 1.15$ nm, where $n=8$ is the number of carbon atoms in the fluorinated blocks. The fully stretched length L_H and the volume V_H of hydrocarbon chains can be calculated according to Tanford's relationship [16]: L_H (nm) $=0.1265m+0.15\approx 2.43$ nm, where $m=18$ is the number of carbon atoms in the hydrocarbon blocks.

The overall F_8H_{18} dipole moment μ_F intensity has been calculated using MOPAC software and found equal to 3.4 D. It is directed along the molecular long axis from the fluorinated chain towards the hydrogenated chain. It is mainly due to the CF_2—CH_2 junction and to the terminal —CF_3 group.

The π-A isotherm diagrams were obtained with a Teflon made Langmuir trough (Riegler and Kirsten). The experiments were performed at $T=20$ °C. The surface pressure was measured continuously using a Wilhelmy plate with an accuracy of about 0.1 mN/m. Monolayers were spread, from a 2.5 mM chloroform F_8H_{18} solution and a 1.0 mM chloroform alamethicin solution, on a pure water surface (pH $=5.7$) and the films were compressed at a constant compression rate of 0.04 nm^2/molecule/min.

The setup used for measurements of x-ray specular reflectivity of liquid surfaces was described elsewhere [17]. The characteristics of the x-ray beam are 0.154 nm for the wavelength λ, about 2×10^6 photons per second for the intensity, 8 mm for the horizontal width w, and 50 μm for the height e. As the x-ray reflectivity is a function of the vertical profile of the mean electron density, it gives information on the molecular packing. Experimental curves are fitted using classical optics with a one-, two-, or three-slab model [18]. The roughness σ of the interface induced by thermal fluctuations is also taken into account. Its contribution to the reflected x-ray intensity is mainly equivalent to a damping term $\exp(-q^2\sigma^2)$ as we discuss in the following, q being the transfer wave vector. According to Daillant *et al.* [19], the diffuse scattering becomes significant when $q^2\sigma^2 \geqslant 1$ and must then be taken into account in the reflectivity data. In this study, this becomes true at about $q=3$ nm^{-1}, which is only at the end of the curves where the reflectivity vanishes. Although introducing the diffuse scattering is more accurate, it adds extra parameters in the theoretical curve; furthermore, the intensity recorded in the specular direction is corrected by the intensity recorded at an angle of 0.1° above the specular direction, in order to subtract not only the background but also a part of the diffuse scattering. Thus, in this study, using a simple damping term $\exp(-q^2\sigma^2)$ gives the same results as taking into account the diffuse scattering. In this case, σ is an effective roughness which takes into account all intrinsic roughnesses and the thermally induced capillary waves. Mean electron densities are derived from the area per molecule A and from the chemical composition and the thickness of the slab. As the molecular area A is determined by the Langmuir trough, the only free parameters of the models are the thickness of the slabs and the roughness.

The mixed alam/F_8H_{18} films were also analyzed using surface potential measurements. Classical Langmuir monolayers can be assimilated generally to arrays of electric dipoles whose density and orientation may change upon compression (see for a review Ref. [21]). The surface potential ΔV of a nonionized monolayer may be calculated, at a given molecular area A, according to the Helmoltz formula $\Delta V=(\mu_\perp)/(\varepsilon_0\varepsilon A)$, where $\mu_\perp$ is the average vertical component of the molecular dipole moment μ, ϵ_0 is the permittivity of the free space, and ϵ is the relative dielectric constant of the monolayer. Basically, the monolayer electric parameter which can be readily deduced from surface potential measurements is the *effective* molecular dipole $\mu_\perp/\varepsilon$. Upon compression, in fact, the surface potential variation ΔV either may originate from reorientation of the electric dipole of the amphiphilic molecules or may result also from the reorientation of water molecules underneath the monolayer. The surface potential (ΔV) versus molecular area A isotherm diagrams were recorded (simultaneously with π-A isotherm diagrams) using a Langmuir trough purchased from Nima Technology Ltd. The surface potential sensor consists of a commercial Kelvin probe with an area of 0.2 cm^2 which is suspended above the film spread at the air-water interface. Surface potential and molecular areas were measured with an accuracy of 30 mV and 5%, respectively.

The mixed films were also transferred onto silicon substrates using the Langmuir-Blodgett (LB) technique, in order to be imaged with an atomic force microscope. The used AFM was a Nanoscope III, and the transferred films were analyzed in the tapping mode.

III. RESULTS

We will first present the structural properties and the dynamic behavior of the pure alam monolayer; then, we will consider, in a second section, the case of mixed alam/F_8H_{18} films.

A. Pure alamethicin monolayer

1. π-A isotherm diagram

Curve *a* of Fig. 1 shows the π-A isotherm diagram of a pure alam monolayer. The steep rise of the π-A isotherm and the compressibility coefficient of 2.9 m/N (at $\pi=20$ mN/m) indicate a solidlike structural organization of the alam monolayer. The molecular area value of 3.2 nm^2 (determined at a surface pressure of 20 mN/m) compares well with the alam molecular dimensions: an alamethicin molecule may be approximated by a cylinder of a 1.0 nm diameter and a 3.0 nm height. These results indicate that the alam molecules are oriented with their α-helix axis parallel to the air-water interface, as shown in a previous study by synchrotron grazing incidence x-ray diffraction (GIXD) experiments [20].

2. Grazing-incidence x-ray reflectivity

In this paper, we report an additional proof of the in-plane orientation of the alam molecules at the air-water interface, using grazing-incidence x-ray reflectivity.

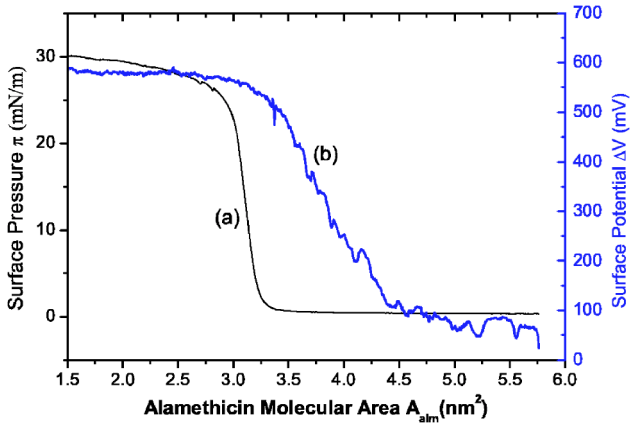

FIG. 1. Surface pressure π (curve *a*) and surface potential ΔV (curve *b*) versus molecular area *A* isotherm diagrams obtained on compressing a pure alamethicin monolayer; the compression speed was about 0.04 nm^2/min/molecule and the temperature was set at $T=20$ °C.

Curve *A* of Fig. 2 shows typical x-ray reflectivity of the pure alam monolayer recorded versus the transfer wave vector *q* at a surface pressure of 20 mN/m and a molecular area of 3.20 nm^2. The profile of the experimental curve is typical for thin monolayers and the data are very well fitted by a one-slab model (see Table I). The measured roughness of 0.28 nm is typical of interfaces with a surface tension of about 50 mN/m. The measured thickness $h_{alam}=0.83$ nm is in agreement with an in-plane orientation of alam molecules at the air-water interface.

We would like to add that the x-ray reflectivity and the measured thickness h_{alam} of the alam monolayer do not vary upon compression in the collapse plateau region. This result is of a particular interest in our study: it shows that the density of the alamethicin monolayer does not change in the collapse plateau region, as corroborated hereafter by surface potential experiments.

3. ΔV-A isotherm diagrams

Curve *b* of Fig. 1 shows the ΔV-*A* isotherm diagram of a pure alamethicin monolayer spread at the air-water interface.

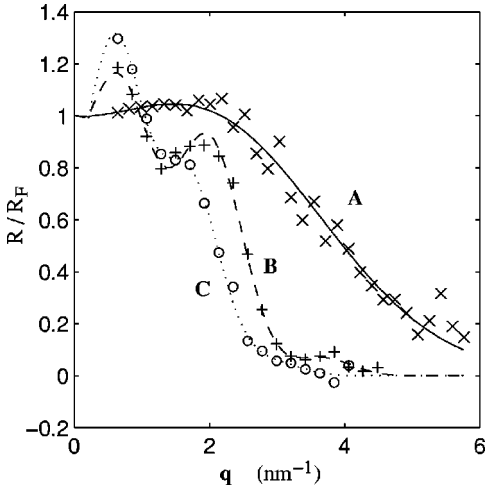

FIG. 2. Experimental reflectivity curves: (curve *A*) a pure alamethicin monolayer compressed at $A_{alam}=3.20$ nm^2 and a mixed F_8H_{18}/alamethicin film compressed to $A_F=0.34$ nm^2 (curve *B*: +) and $A_F=0.28$ nm^2 (curve *C*: O). For curve *A*, the solid line corresponds to the best fit using a one-slab model. Solid lines correspond to the best fits of the experimental curves whose parameters are presented in Table I.

Upon compressing, the alam monolayer exhibits an abrupt increase in surface potential at a molecular area of about 4.0 nm^2; then, ΔV reaches a value of about 0.540 V in the alamethicin solid 2D phase, at $A_{alam}=3.20$ nm^2. We would like to note that the occurrence of a sudden jump in surface potential isotherm diagrams is typical for many amphiphilic monolayers. It is generally attributed to a sudden decrease of the monolayer dielectric constant ϵ due to (i) an aggregation process of growing domains of the dense phase during the gas-dense phase transition and (ii) and to the subsequent expelling of water molecules from the headgroups-subphase interface [22].

As we showed above, alamethicin molecules lay with their long helix axis parallel to the air-water interface; hence, the measured surface potential ΔV is proportional to the normal component $\mu_{alam,\perp}$ of the alam electric dipole moment relative to the long axis of its helix. The positive sign of the recorded ΔV shows that $\mu_{alam,\perp}$ is oriented upwards—i.e.,

TABLE I. Fits parameters values of two experimental x-ray reflectivity curves recorded for a mixed F8H18/alamethicin film with $R_{F/alam}=3.94$ [see Figs. 2 (*B*) and (*C*)] and for a pure alamethicin monolayer [see Fig. 2 (*A*)]. Experimental curves of the mixed film were recorded at $A_F=0.34$ nm^2 and $A_F=0.28$ nm^2. The best models are HF_2H and FH model (see Fig. 4). For the FH model, the fluorinated slab thickness was limited to $L_F=1.25$ nm; h_1, h_2, and h_3 represent, respectively, the thickness of the upper, medium and lower slab; h_{alam} represents the thickness of the lower alamethicin monolayer. Experimental curve of the pure alamethicin monolayer film was recorded at $A_{alam}=3.20$ nm^2 and a surface pressure of 20 mN/m.

	Model	h_1 (nm)	h_2 (nm)	h_3 (nm)	h_{alam} (nm)	σ (nm)	χ^2
$A_F=0.34$ nm^2	HF_2H	0.83	1.36	0.90	0.73	0.51	0.18
	FH	0.93	1.59	–	0.71	0.62	0.85
$A_F=0.28$ nm^2	HF_2H	1.05	1.45	1.12	0.65	0.67	0.21
	FH	1.25	1.74	–	0.71	0.80	0.65
$A_{alam}=3.20$ nm^2 (pure alamethicin monolayer)					0.83	0.28	0.32

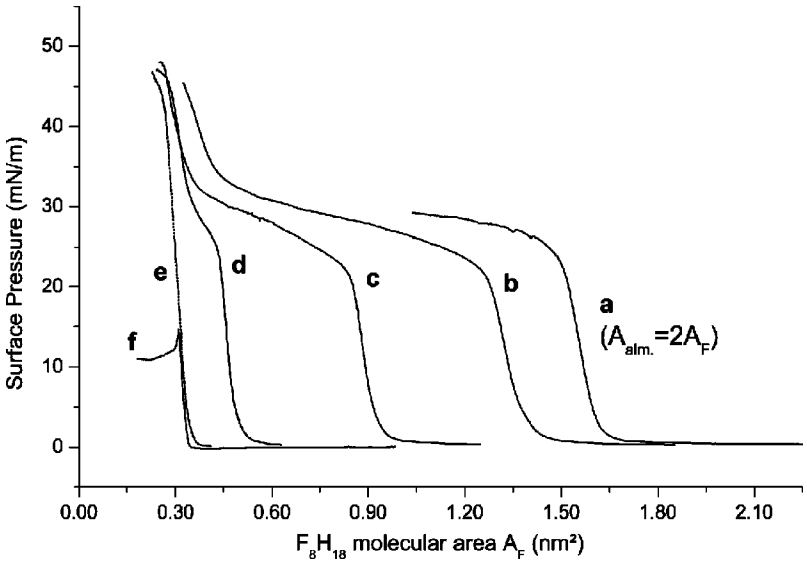

FIG. 3. Surface pressure π versus A_F molecular area isotherm diagrams, obtained on compressing mixed films of F_8H_{18}/alamethicin made with different molecular mixture ratios $R_{F/alam}$; the compression speed was about 0.04 nm2/min/molecule and the temperature was set at $T=20\,^{\circ}C$. Curve *a*: pure alamethicin monolayer. Curve *b*: $R_{F/alam}=2.46$. Curve *c*: $R_{F/alam}=3.68$. Curve *d*: $R_{F/alam}=7.06$. Curve *e*: $R_{F/alam}=11.06$. Curve *f*: pure F_8H_{18} monolayer. To convert the *x* axis from A_F values to A_{alam} values, one should multiply A_F values by $R_{F/alam}$ (except for curve *a* for which A_F values should be multiplied by 2).

from the water subphase towards the air. Applying the Helmoltz formula for $\Delta V=540$ mV and $A_{alam}=3.20$ nm^2, one could deduce $\mu_{alam,\perp}/\varepsilon=4.62$ D. The transverse component of the alam electric dipole moment which appears to be much smaller than the parallel component as reported in the literature [23]: $\mu_{alam,\perp}=75$ D. One should remark that the measurement of such an electric dipole moment could originate from either (i) a genuine transverse electric dipole moment which would be oriented from the hydrophilic "side" towards the hydrophobic "side" of the alamethicin helix or (ii) a slight tilt of the long axis of alamethicin molecules.

On compressing further the alamethicin monolayer in the collapse region, the surface potential remains constant. This result is in agreement with our previous statement that the alam monolayer density remains constant during the collapse process. We think that the collapse of alamethicin monolayer corresponds to a solubilization of molecules in the water subphase.

B. Mixed alamethicin-F_8H_{18} films

Generally, in the case of mixed films made of two classical amphiphilic molecules, the molecular area *A* used to plot π-*A* isotherm diagrams is the average molecular area of the two used amphiphilic molecules, as the two amphiphilic species share the same surface. In our particular case, we define two molecular areas, A_F for F_8H_{18} and A_{alam} for alamethicin, by dividing the overall film area *S* by the number of either F_8H_{18} molecules (n_F) or alamethicin molecules (n_{alam}): $A_F=S/n_F$ and $A_{alam}=S/n_{alam}$. We define also $R_{F/alam}=n_F/n_{alam}$ as the F_8H_{18}/alam molecular mixture ratio.

To convert the π-*A* isotherm diagram *x* axis from A_F to A_{alam}, one should simply multiply A_F values by the considered $R_{F/alam}$ value.

1. π-A isotherm diagrams

Curves *b*–*f* of Fig. 3 show the surface pressure π-*A* isotherm diagrams of mixed alam/F_8H_{18} films as a function of A_F for different $R_{F/alam}$ values.

According to these π-*A* isotherm diagrams, one may note the following.

(i) The film can be compressed up to surface pressure values of about 45 mN/m, which is greater than the sum of the individual collapse pressure values of both F_8H_{18} and alamethicin pure monolayers, respectively, $\pi_{c,F}=12$ mN/m and $\pi_{c,alam}=29$ mN/m.

(ii) The surface pressure π increases steeply at an alamethicin molecular area A_{alam} of about 3.2 nm^2 as for the pure alamethicin monolayer (curve *a*).

These results indicate that F_8H_{18} and alamethicin molecules do not share the same surface.

After the continuous collapse of the alamethicin monolayer, a second increase in π occurs practically at a molecular area value of about $A_F\sim0.3$ nm^2, which is equal to the molecular area A_{F_0} of a pure and dense semifluorinated monolayer (curve *f* of Fig. 3). Thus, the second increase in π should be attributed to the compressing of a monolayer of F_8H_{18} molecules alone. It is in agreement with our statement that F_8H_{18} and alamethicin molecules lay at two different interfaces.

A particular case is where $R_{F/alam}=11.06$ (curve *e* of Fig. 3) for which the surface pressure increases steadily from 0 mN/m up to 45 mN/m at a molecular area of about 0.3 nm^2. For this particular value of $R_{F/alam}$, one may expect that the underlying alam monolayer should be fully covered by F_8H_{18} molecules. Indeed, in this case, the molecular mixture ratio can be expressed also as $R_{F/alam}=A_{0,alam}/A_{F_0}$, where $A_{0,alam}=3.20$ nm^2 and $A_{F_0}=0.28$ nm^2 represent molecular areas of the close packed pure alam and F_8H_{18} monolayers, respectively.

Also, we would like to remark that in the case of curve *b* of Fig. 3, which corresponds to a small $R_{F/alam}=2.46$ value, the second increase in surface pressure occurs at a molecular area $A_F\sim0.35$ nm^2 which is sensitively greater than A_{F_0}. Nevertheless, due to the small surface of the Langmuir trough and to the large difference between molecular areas of alamethicin and of F_8H_{18} molecules, the observed difference between curve *b* and the other curves of Fig. 3 should be attributed actually to a greater error in the calculation of

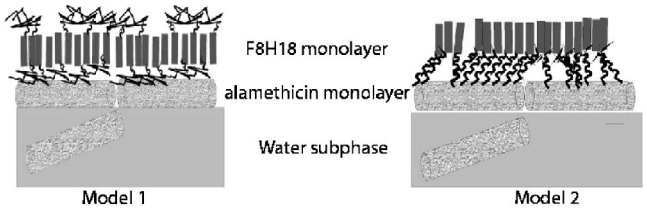

FIG. 4. Schematic representation of two possible models for the orientation of the upper F_8H_{18} monolayer: HF_2H (model 1) or FH (model 2). Whereas both models can be accepted by regards to GIXR data, the HF_2H which suggests the formation of a nonpolar F_8H_{18} monolayer should be rejected according to surface potential measurements.

molecular areas. In this case also, border effects should be greater.

From the above observations, one may conclude that the first increase in surface pressure corresponds to the compression of a homogeneous and pure monolayer of alamethicin molecules and the second increase of surface pressure corresponds to the compression of a homogeneous and pure monolayer of F_8H_{18} molecules. Such a result means also that F_8H_{18} molecules forms spontaneously a monolayer on the top of the alamethicin monolayer; i.e., F_8H_{18} and alamethicin molecules demix spontaneously along the normal to the air-water interface.

2. Grazing-incidence x-ray reflectivity

Figures 2 (*B*) and (*C*) show experimental x-ray reflectivity curves obtained for a mixed F_8H_{18}/alamethicin film with $R_{F/alam}=3.94$, recorded, respectively, at two A_F values where a homogeneous dense phase of F_8H_{18} molecules is expected: $A_F=0.34$ nm^2 ($\pi=27$ mN/m) and $A_F=0.28$ nm^2 ($\pi=45$ mN/m). These experimental data have been fit using the same models used in a previous study on F_8H_{18} Langmuir films [12,13]: FH/HF, FH, HF, HF_2H, and FH_2F. In the first model, SFA molecules orient themselves antiparallel relative to each other on the alametihicin monolayer; this is a two-slab model that has only three parameters (two thicknesses and the effective roughness). In the second one, the FH monolayer model, the fluorinated chains extend upward and the hydrocarbon chains extend downward—i.e., toward the alamethicin monolayer; it has four parameters. In the third model, HF, the fluorinated chains are downward and the hydrocarbon chains are upward; it also has four parameters. The two remaining HF_2H and FH_2F models consist of interleaved bilayers on the alamethicin monolayer (see Fig. 4) and have five parameters.

Parameters values of the best fits (for which $\chi^2 \leqslant 1$) are reported in Table I. FH_2F, HF, and FH/HF models are rejected because, for acceptable slab thicknesses, their χ^2 values are well above 1: approximately 5, 8, and 500, respectively. The best fitting models were found to be FH and HF_2H at $A_F=0.34$ nm^2 and $A_F=0.28$ nm^2 (see Fig. 2).

The effective roughness is found to be between 0.5 and 0.8 nm. This is larger than expected: For a surface tension about 40 mN/m, which is the value for the film around $A_F=0.3$ nm^2, the expected roughness σ is about 0.35 nm when one only takes into account the thermally induced capillary waves ($\sigma \propto \gamma^{-1/2}$, where γ is the surface tension). Actually, there is not one but three interfaces (water/alamethicin, alamethicin/F_8H_{18}, and F_8H_{18}/air) and some preliminary GIXD data show that the alamethicin/F_8H_{18} interface is rough; furthermore, defects, such as holes in the film or inhomogeneities are likely to be present in the film (F_8H_{18} is known to exhibit unusual packing in films [12]). All this increases substantially the effective roughness of the film. The main consequence for that high effective roughness is that there is strong diffuse scattering by the film, and the x-ray reflectivity vanishes rapidly, as can be seen on Fig. 2. In this case a more precise theory that takes into account diffuse scattering should have been used. But the same results were found using both theories (see the experimental section); this is essentially due to our experimental procedure, where the diffuse scattering intensity is partly removed from the raw reflectivity data. Another consequence of that large effective roughness is that the thickness found for the alamethicin layer is only indicative, as it is not large compared to the roughness (see Table I).

For the FH model, the measured thicknesses of the fluorinated and the hydrocarbon slabs were found, respectively, equal to 0.93 nm and 1.59 nm at $A_F=0.34$ nm^2. For data recorded at $A_F=0.28$ nm^2, the hydrocarbonated slab thickness was found about 1.74 nm with a restricted maximum value of about $L_F=1.25$ nm for the fluorinated slab thickness.

Using the HF_2H model, the measured thickness of the inward fluorinated slab was found equal to 1.36 nm and 1.45 nm for $A_F=0.34$ nm^2 and $A_F=0.28$nm^2, respectively. These values, which are slightly higher than the maximum value L_F, should not be rejected since the fluorinated chains may be slightly shifted relative to each other. The thickness of the external hydrocarbon leaflets were found to be approximately equal to 0.86 nm and 1.08 nm for $A_F=0.34$ nm^2 and $A_F=0.28$ nm^2, respectively.

The thickness of the alamethicin sublayer was found close to the one measured in the case of a pure monolayer of alamethicin molecules for both FH and HF_2H models.

Hence, x-ray reflectivity experiments give an additional evidence of the formation of two monolayers stacked over each other. Nevertheless, our x-ray data do not allow for choosing between the two models.

3. Atomic force microscopy

In order to have a better view of the molecular organisation of the mixed alam/F_8H_{18}, we used the Langmuir Blodgett technique to transfer, onto silicon substrates, single layers of the mixed alam/F_8H_{18} film at different surface pressure values.

Figure 5(a) shows an AFM image of one alam/F_8H_{18} layer transferred at 24 mN/m and a large A_F value of about 0.6 nm^2. Analysis of this image shows that F_8H_{18} molecules form nanoscopic circular domains with a characteristic size of about 4.0 nm and a thickness approximately equal to 2.6 nm. This latter value is rather in agreement with the FH model. At a smaller A_F value of about 0.3 nm^2, a close-packed monolayer of F_8H_{18} molecules with a similar nanoscopic pattern can be observed [Fig. 5(b)].

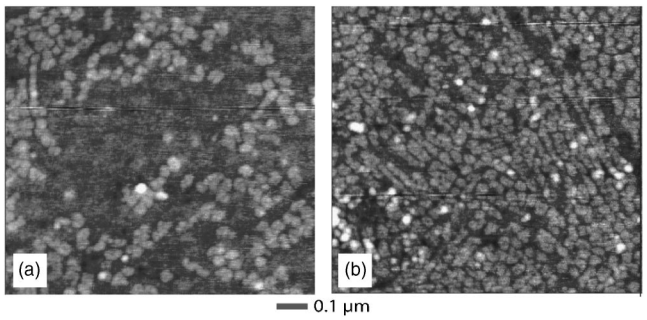

FIG. 5. AFM images of two single alam/F_8H_{18} mixed layers transferred at: (a) $A_F=0.6$ nm^2, the F_8H_{18} monolayer occupy roughly half of the overall surface as expected, (b) $A_F=0.3$ nm^2, an almost densily packed monolayer of F_8H_{18} molecules can be observed.

4. Surface potential measurements

Figures 6(a) and 6(b) show the ΔV-A isotherm diagrams of two alam/F_8H_{18} mixed films with $R_{F/alam}=2.50$ and $R_{F/alam}=3.68$, respectively.

As we can notice, the greater the density of the upper F_8H_{18} monolayer, the lower the surface potential of the mixed film. Hence, since the surface potential of a pure alam monolayer is positive (curve *b* of Fig. 1), such a result indicates that the surface potential of the upper F_8H_{18} monolayer is negative. Thus F_8H_{18} molecules should orient their electric dipole moment downward. Consequently, one should reject the HF_2H model and consider the FH model.

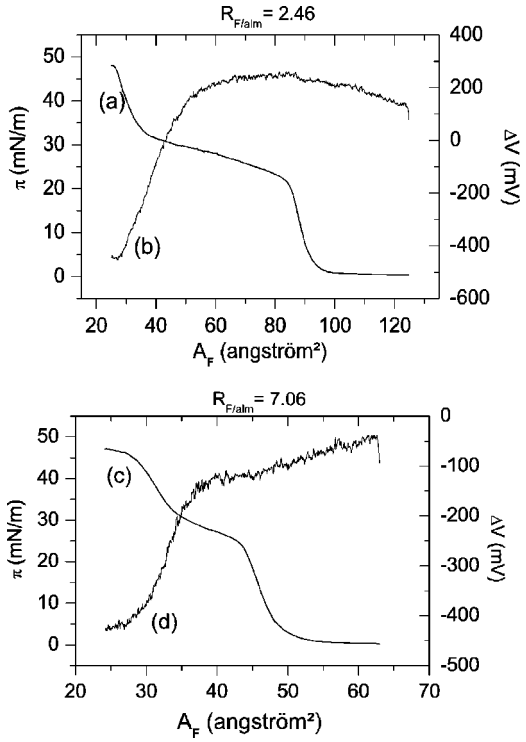

FIG. 6. Surface pressure π (curve *a*) and Surface potential ΔV (curve *b*) versus molecular area A_F isotherm diagrams of a F_8H_{18}/alamethicin mixed film made with a molecular ratios $R_{F/alam}=7.06$; the compression speed was about 0.04 nm^2/min/molecule and the temperature was set at $T=20$ °C. To convert the x axis from A_F values to A_{alam} values, one should multiply A_F values by $R_{F/alam}$ values.

Moreover, a plot of ΔV vs A_F^{-1} (Fig. 7) measured at a fixed $A_{alam}=3.20$ nm^2 shows clearly a linear decrease of ΔV versus the density of the F_8H_{18} upper layer. In order to explain this linear decrease, let us consider the F_8H_{18}/alamethicin bilayer as a two layers capacitor with two different electric dipole moments and two different dielectric constants: $\mu_1=\mu_{alam}$, $\varepsilon_1=\varepsilon_{alam}$ and $\mu_2=\mu_F$, $\varepsilon_2=\varepsilon_F$ for the alamethicin and the F_8H_{18} layers, respectively. Thus one could write, by analogy with the Demchak model [24],

$$\varepsilon_0 \Delta V = \frac{\mu_1}{\varepsilon_1 A_1} + \frac{\mu_2}{\varepsilon_2 A_2}.$$

Considering the experimental value of the surface potential of the alamethicin monolayer,

$$\frac{\mu_1}{\varepsilon_1} = 4.62 \text{ D}.$$

At $A_1=A_{alam}=3.20$ nm^2, the above equation becomes

$$\Delta V = 0.54 + \frac{1}{2.65}\left(\frac{\mu_2}{\varepsilon_2}\right)\frac{1}{A_2},$$

where ΔV, μ_2, and A_2 are expressed in volt, debye, and nm^2, respectively.

The determination of the experimental slope of the linear curve ΔV vs A_F^{-1} gives an estimation for the effective electric dipole of F_8H_{18} molecules:

$$\frac{\mu_F}{\varepsilon_F} = -0.78 \text{ D}.$$

Moreover, if one considers the calculated value of $\mu_F=3.4$ D and a value of about 4.5 for the dielectric constant of the F_8H_{18} monolayer, as reported by Hariharan and Harris [25] for F_6H_6, then one may deduce a calculated value of $\mu_F/\varepsilon_F=-0.75$ D, which is a close agreement with the experimental value −0.78 D.

IV. DISCUSSION

Previously, Krafft *et al.* [26] showed the occurrence of a vertical phase separation in mixed Langmuir films made of another semifluorinated alkane—namely, F_8H_{16}—and a phospholipid (DPPE). However, their reported vertical phase separation was observed only at surface pressure values equal or higher than the collapse surface pressure of the pure semifluorinated monolayer—i.e., $\geqslant$13 mN/m, whereas at lower surface pressure values a lateral "miscibility" is observed. Actually, the spreading at the air-water interface of F_8H_{16} molecules (which carry no hydrophilic headgroups), despite the presence of a more suitable DPPE/air interface, may indicate that the behavior of the F_8H_{16}/DPPE system

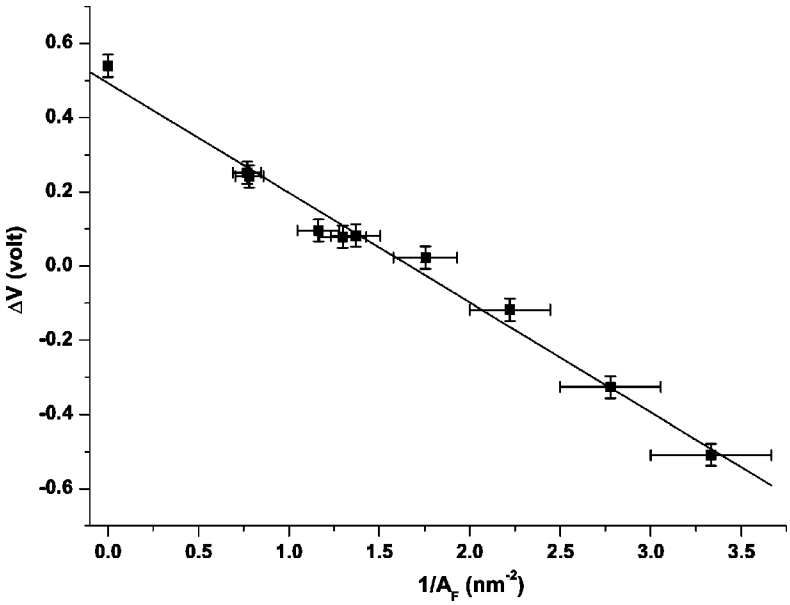

FIG. 7. Plot of surface potential ΔV versus A_F^{-1}. The different values of ΔV were measured from different mixed F_8H_{18}/alamethicin films at a fixed alamethicin molecular area of $A_{alam} = 3.20$ nm^2, with $R_{F/alam}$ varying from 0 to 11.

should be mainly governed by minimization of the air-water interface surface tension ($\gamma_{A/W}$).

The ability of semifluorinated molecules to form monolayers either on the water surface or on hydrophobic surfaces shows that the lateral SFA-SFA interactions play a key role in the spreading behavior of SFA and the stabilizing of their monolayers. They also lead generally to the self-aggregation of SFA in nanoscopic domains or, in some particular cases, to their insertion in hydrophobic cavities, as reported by Lo Nostro in a recent study [27] on mixed films of F_8H_{16} and cyclodextrin.

Moreover, since semifluorinated alkanes carry a strong electric dipole, the determination of the molecular orientation of the upper SFA monolayer may give a valuable insight into the nature of the stabilizing lateral interactions. For example, strong electrostatic interactions and long hydrocarbon blocks should favor HF_2H organization whereas long fluorinated blocks should favor FH organization. Such a statement is confirmed by a new study we are currently carrying out on another mixed film made of $F_{10}H_{10}$ and alamethicin. Preliminary results show that $F_{10}H_{10}$ adopt on the top of the alam monolayer a parallel FH orientation at large molecular areas, whereas at smaller molecular areas, they adopt the antiparallel HF_2H orientation. These results will be discussed in more detail elsewhere.

V. CONCLUSION

We investigated an experimental method to study the dynamic behavior of semifluorinated alkanes on hydrophobic surfaces versus lateral compression. We have shown, in particular, that the F_8H_{18} diblock semifluorinated alkane spreads spontaneously on the top of an amphiphilic Langmuir monolayer made of the natural alamethicin peptide. Thanks to the suitable structure and the collapse properties of the underlying monolayer, the upper semifluorinated monolayer can be compressed continuously until a dense monolayer is obtained. Combining results of surface pressure (π) versus molecular area A measurements, grazing-incidence x-ray reflectivity measurements, atomic force microscopy observations, and surface potential (ΔV) versus molecular area A measurements allow for the discrimination between different possible orientations of F_8H_{18} molecules and also for the determination of the dielectric constant of the semifluorinated monolayer value.

[1] J. F. Rabolt, T. P. Russell, and R. Twieg, Macromolecules **17**, 2786 (1984).
[2] W. Mahler, D. Guillon, and A. Skoulios, Mol. Cryst. Liq. Cryst., Lett. Sect. **2**(3-4), 111 (1985).
[3] C. Viney, T. P. Russell, L. E. Depero, and R. J. Twieg, Mol. Cryst. Liq. Cryst. **63**, 168 (1989).
[4] J. Höpken and M. Möller, Macromolecules **25**, 2482 (1992).
[5] G. L. Gaines, Jr., Langmuir **7**, 3054 (1991).
[6] B. P. Binks, P. D. I. Fletcher, S. N. Kotsev, and R. L. Thompson, Langmuir **13**, 6669 (1997).
[7] P. Marczuk, P. Lang, and M. Möller, Colloids Surf., A **163**, 103 (2000).
[8] Y. Hayami and H. Sakamoto, Colloid Polym. Sci. **282**, 461 (2004).
[9] G. Gaines, Jr., *Insoluble Monolayers at Liquid-Gas Interfaces* (Interscience, New York, 1996).
[10] Z. Huang, A. A. Acero, N. Lei, S. Rice, Z. Zhang, and M. Schlosmann, J. Chem. Soc., Faraday Trans. **92**, 545 (1996).
[11] A. El Abed, E. Pouzet, M.-C. Fauré, M. Sanière, and O. Abillon, Phys. Rev. E **62**, R5895 (2000).
[12] A. El Abed, M.-C. Fauré, E. Pouzet, and O. Abillon, Phys. Rev. E **65**, 51603 (2002).

[13] M. Maaloum, P. Muller, and M.-P. Krafft, Angew. Chem., Int. Ed. **41**, 4331 (2002).
[14] P. Lo Nostro, Curr. Opin. Colloid Interface Sci. **8**, 223 (2003).
[15] P. Lo Nostro and S. H. Chen, J. Phys. Chem. **97**, 6535 (1993).
[16] C. Tanford, *The Hydrophobic Effect: Formation of Micelles and Biological Membranes*, 2nd ed. (Wiley, New York, 1980), p. 52.
[17] C. Postel and O. Abillon, Langmuir **14**, 5649 (1998).
[18] M. Born and M. Wolf, *Principles of Optics*, 6th ed. (Pergamon, New York, 1991), Chap. 1.6.
[19] J. Daillant and O. Belorgey, J. Chem. Phys. **97**, 5824 (1992); J. Daillant and M. Alba, Rep. Prog. Phys. **63**, 1725 (2000).
[20] R. Ionov, A. El Abed, A. Angelova, M. Goldmann, and P. Peretti, Biophys. J. **78**, 3026 (2000).
[21] D. M. Taylor, Adv. Colloid Interface Sci. **87**, 183 (2000).
[22] O. Oliveira, Jr. and C. Bonardi, Langmuir **13**, 5920 (1997).
[23] S. Stankowski, U. D. Schwarz, and G. Schwarz, Biochim. Biophys. Acta **11**, 941 (1988).
[24] R. J. Demchak and T. J. Fort, Jr., J. Colloid Interface Sci. **46**, 191 (1974).
[25] A. Hariharan and J. G. Harris, J. Chem. Phys. **101**, 4151 (1994).
[26] M. P. Krafft, F. Giulieri, P. Fontaine, and M. Goldmann, Langmuir **17**, 6577 (2001).
[27] P. Lo Nostro, A. Santoni, M. Bonini, and P. Baglioni, Langmuir **19**, 2313 (2003).